Sustainable Chemistry and Pharmacy 49 (2026) 102315

Contents lists available at ScienceDirect

Sustainable Chemistry and Pharmacy

journal homepage: www.elsevier.com/locate/scp

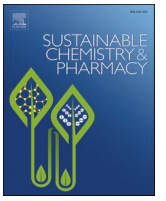

Recyclable Brønsted-Lewis acidic ionic liquids enable high-yield biomass valorization to platform chemicals in aqueous biphasic systems☆

Winifred D. Anyomih [a], James Darkwa [a], Paseka T. Moshapo [a], Gift Mehlana [b], Banothile C.E. Makhubela [a,*]

[a] Research Centre for Synthesis and Catalysis, Department of Chemical Sciences, Faculty of Science University of Johannesburg, Auckland Park Kingsway Campus, Auckland Park, 2006, Johannesburg, South Africa
[b] Department of Chemical Sciences, Midlands State University, 9055 Senga Road, Gweru, Zimbabwe

ARTICLE INFO

Keywords:
Ionic liquids
Furfural
Levulinic acid
(Hemi)cellulose
Waste biomass conversion
Green chemistry

ABSTRACT

Multiple product formation in biorefineries maximizes biomass valorization, resource efficiency, process integration, and flexibility in adapting to fuels, chemicals, and materials demand. We report a Brønsted acidic (BAIL) and Brønsted-Lewis acidic ionic liquids (BLAILs) that promote tandem biphasic extraction-conversion-separation of levulinic acid (LA), 5-hydroxymethylfurfural (HMF) and furfural (FFR) from (hemi)cellulose in corn cobs and giant cane biomass. Reacting 1-benzyl-1H-imidazole and 1,4-butane sultone, afforded 1-benzyl-3-(4-sulfonatobutyl) imidazolium (zwitterion **1**). This was followed by protonation of zwitterion **1**, leading to 1-benzyl-3-(4-sulfobutyl)-1H-imidazole-3-ium (BAIL **2**), which was treated, separately, with $FeCl_3$, $ZnCl_2$, $SnCl_2$, and $NiCl_2$ to give BLAILs (**3a-d**) with larger anions ($FeCl_4^-$, $ZnCl_3^-$, $SnCl_3^-$, and $NiCl_3^-$). These IL catalysts mediated raw biomass conversion *via* extraction-hydrolysis-dehydration and separation of FFR, LA and HMF. Under optimized conditions, BAIL (**2**) achieved 91 % FFR yield, while the BLAIL, incorporating $FeCl_4^-$, yielded 95 % FFR. The sequence of the BLAILs' catalytic activity, which corresponded to their Lewis acidities, was $FeCl_4^- > SnCl_3^- > ZnCl_3^- > NiCl_3$. Post-reaction solid residues characterized using SEM, PXRD, and FT-IR, revealed significant structural changes in biomass, including increased crystallinity, attributed to type I microcrystalline cellulose. This work establishes an efficient, high-yielding, and selective method for converting and separating FFR, HMF, LA, and pure microcrystalline cellulose from biomass using recyclable, earth-abundant metal-based ILs.

1. Introduction

Burning non-renewable fossil fuels and their products is often associated with emitting toxic and greenhouse gases like carbon dioxide (CO_2), methane (CH_4), oxides of nitrogen (NO_x), oxides of sulfur (SO_x), and fluorinated gases that contribute to environmental deterioration. This is a recurring global concern that has resulted in scientists looking for alternative, cleaner options to fossil fuels

☆ In loving memory of Novisi Komla Oklu, who remains forever in our hearts. This work is for you.

* Corresponding author.
E-mail addresses: pasekam@uj.ac.za (P.T. Moshapo), bmakhubela@uj.ac.za (B.C.E. Makhubela).

https://doi.org/10.1016/j.scp.2026.102315
Received 7 October 2025; Received in revised form 7 January 2026; Accepted 8 January 2026

(Kumar et al., 2024; Li et al., 2024). As such, in the past decade, renewable carbon sources like lignocellulosic biomass, a carbon-neutral and sustainable source of carbon for producing bio-based fuels and chemicals (Wu et al., 2024), have been the subject of interest for the production of biofuels and chemicals through biorefinery processes (Shuai and Luterbacher, 2016). Lignocellulose, found in plant biomass, is the most abundant and renewable second-generation biomass feedstock (Segers et al., 2024). Comprising cellulose, hemicellulose, and lignin (with trace amounts of ash, proteins, and oils), this carbon source can be (Shuai and Luterbacher, 2016) hydrolyzed to afford sugars like xylose and glucose. Xylose serves as the main precursor to furfural (FFR) production through acid-catalyzed or hydrothermal xylose dehydration reactions (Topias Kilpinen et al., 2024). While glucose yields 5-hydroxymethylfurfural (HMF), which can further yield levulinic acid (LA) from subsequent rehydration of HMF under acidic conditions (Thanheuser et al., 2024). The reversible glucose-to-fructose isomerization, known as the Lobryede-Bruynevan-Ekenstein transition, is crucial for the high-yield synthesis of HMF from glucose (Liu et al., 2024). These compounds have been identified as part of Bozell and Peterson's updated list of platform compounds (de Jong et al., 2020). FFR can be upgraded to fuels and chemicals such as FFR alcohol (FFA), 2-methylfuran (MF), ethyl levulinate (EL) and γ-valerolactone (GVL) (Topias Kilpinen et al., 2024), which can be obtained through several reactions, including hydrogenation and oxidation reactions (Topias Kilpinen et al., 2024; Ahmad et al., 2022).

Industrial processes like the Quaker Oats (Lange and Wadman, 2020) and the Biofine Process (Kapanji et al., 2021) utilize sulfuric acid to produce high yields of FFR and LA (Hayes et al., 2006). However, it is highly corrosive and toxic, posing challenges including equipment corrosion, high water consumption, the generation of harmful vapours, ineffective and costly separation procedures and acid effluents (Vojtova et al., 2024). To address this, heterogeneous acid catalysts such as zeolites (Torres-Olea et al., 2024; Wang et al., 2022; Karinen et al., 2011), alumina (Weingarten et al., 2011; You et al., 2014), heteropolyacids (Guo et al., 2018; Liu et al., 2020; Zhang et al., 2019), MCM-41 (Olivares et al., 2023)' (Hu et al., 2024) have been explored for producing FFR and LA, offering easier catalyst separation from the reaction mixture. Nonetheless, humins and other polymeric substances promoted by the condensation and resinification of platform chemicals and/or sugars block the active sites of these catalysts, minimising their durability and effectiveness over time. This has prompted interest in greener alternatives (Tran et al., 2017; Cheng et al., 2021).

In recent years, ionic liquids (ILs) have been used in biorefinery due to their unique and tunable properties (Singh et al.), including their high thermal stability, low volatility, low melting point, and insignificant vapour pressure (Radhakrishnan et al., 2021), making them appropriate for use as solvents, catalysts, or even both in a reaction (Karami et al., 2019) (Oklu et al., 2020). Acidic ILs, particularly imidazolium-based ones, can effectively dissolve biomass (Singh et al.); as such, they are the subject of many studies (Green and Long, 2009). ILs can have either Lewis, Brønsted acidic or a combination of both acidic characteristics (Amarasekara, 2016). Sulfonic acid groups are usually anchored on the cation of the ILs to enhance their Brønsted acidity. For example, 1-methyl-3-(3-sulfopropyl) imidazolium hydrogen sulfate afforded FFR in 85 % and 73 % yields, respectively, from hemicellulose and sugar cane bagasse (Matsagar and Dhepe, 2017). While Ren et al. produced 44.5 % LA from cellulose using $[C_3SO_3Hmim]HSO_4$ (Ren

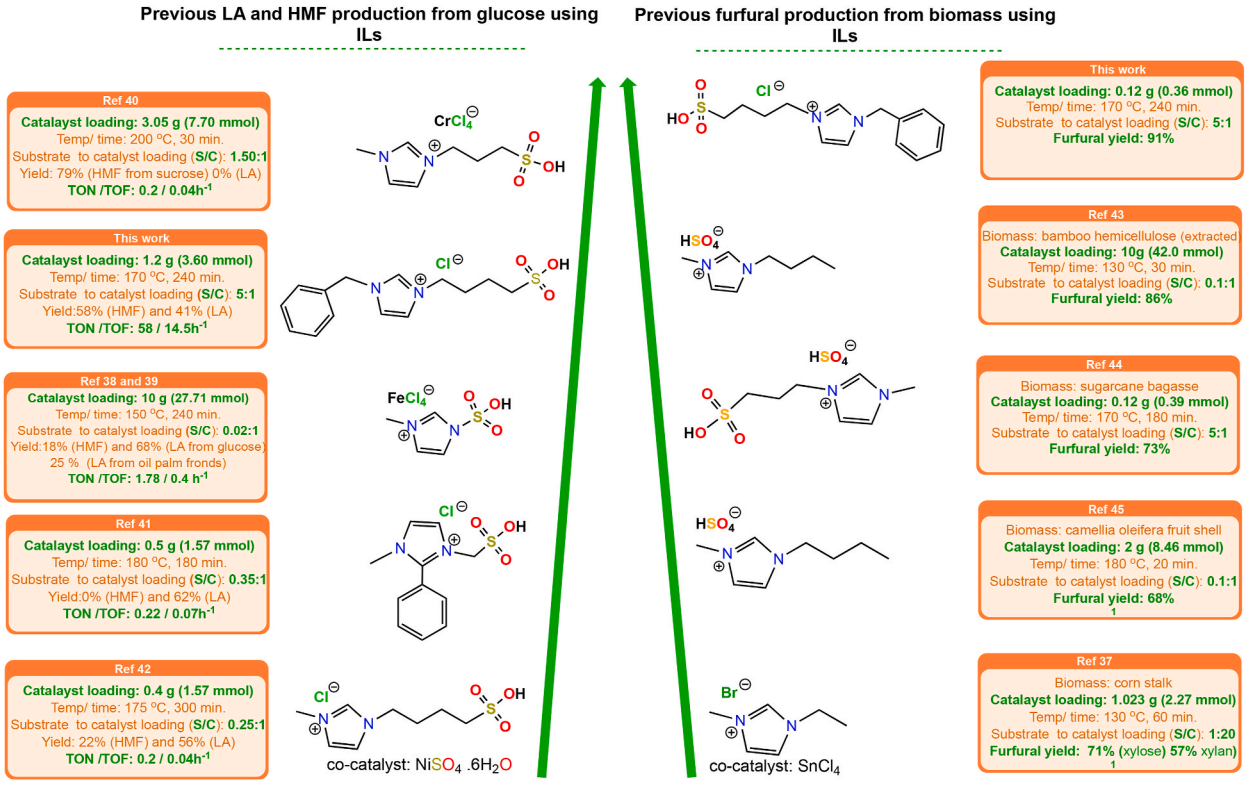

Scheme 1. Comparison of different IL catalysts' performance on the conversion of biomass to FFR, LA and HMF.

et al., 2013).

Dual-functionalized ILs containing Brønsted and Lewis acid centres (BLAIL) provide multiple acidic functionalities that enhance their catalytic and solvating properties in biorefinery (Chang et al., 2018). For instance, when 1-ethyl-3-methylimidazolium bromide (EMIMBr) with $SnCl_4$ co-catalyst was used, FFR yields of 71 % and 55 % were obtained from xylose and cornstalks, respectively (Scheme 1) (Nie et al., 2019). Additionally, a yield of 69.2 % and 24.8 % of LA has been produced from glucose and oil palm fronds using [SMIM][$FeCl_4$] (Ramli and Amin, 2017; Aainaa et al., 2015). Using the Brønsted-Lewis IL [HO_3S–$(CH_2)_3$–mim]Cl–$CrCl_3$ as a catalyst, Yao et al. reported a 78.8 % yield of HMF from sucrose (Yao et al., 2016). Overall, comparing the reaction conditions of earlier BAIL and BLAIL catalysts (Scheme 1; Table S4–S7), these systems generally require substantially higher catalyst loadings to achieve conversion of substrates to LA, HMF, and FFR. In contrast, the BAIL **2** and BLAIL catalysts reported in this work operate at eight times lower catalyst loadings yet deliver markedly higher substrate conversion per millimole of catalyst. This translates into record-high turnover numbers (TONs) and enhanced catalyst productivities (Kumar et al., 2020, 2021; Xia et al., 2023; Matsagar et al., 2017; Huang et al., 2022) (See Scheme 1).

Although there are concerns about the toxicity and biodegradability of the IL, several commercial processes have demonstrated safe and sustainable use of ILs (Costa et al., 2017; Greer et al., 2020). This raises the need to use ILs in catalytic amounts and not as bulk solvents to lessen their toxicity to the environment, the difficulty in handling and overall costs in processes developed with ILs (Fliegar and Flieger, 2020). Moreover, process intensification through reduced reaction steps and tandem-type catalytic reactions - in a one-pot system-can aid in making biorefineries greener and cost-efficient (Arias et al., 2024; Haldar et al., 2022).

We report a high-yielding method for converting raw biomass directly into FFR, HMF and LA in a biphasic tandem extraction-conversion-separation reaction, employing imidazolium ILs with sulfonic and Lewis acid moieties. While several studies show ILs can produce individual platform chemicals (like HMF, LA and FFR) from lignocellulose, simultaneous production of these platform chemicals (plus micro- or nano-crystalline cellulose) with the benefit of tandem separation of the product in aqueous biphasic media can be beneficial and is presented herein.

2. Results and discussion

2.1. Synthesis of ionic liquids

The imidazolium-based Brønsted Acidic Ionic Liquid (BAIL **2**) used in this study was synthesized by reacting benzyl imidazole with 1,4-butane sultone to form a zwitterionic (**1**), which was then treated with hydrochloric acid, and a viscous ionic liquid (**2**) was formed. Lewis acids were incorporated into the BAIL (**2**) to form the BLAILs (**3a-3d**). The synthesis and products are summarized in Scheme 2. The ILs were characterized using advanced spectroscopic and analytical techniques, including 1-D and 2-D NMR spectroscopy, infrared spectroscopy and high-resolution electrospray ionization mass spectroscopy (HR-ESI-MS). Physical properties such as viscosity and Hammett acidity (H_0) were also determined.

2.2. Characterization of ionic liquids

Mass spectra (MS) show peaks that correspond to the cationic species of the ionic liquids in the positive ionization mode with a calculated mass-to-charge (m/z) of 295.1111 for $[C_{14}H_{19}SN_2O_3]^+$ $[M]^+$, and an observed value of m/z = 295.1115. In the negative ionization mode, the corresponding anionic species was detected with a calculated m/z of 329.0732 $[M\text{-}H]^-$ for $[C_{14}H_{19}SN_2O_3Cl]^-$ and an observed m/z of 329.0715. The m/z values and relative abundances of the BLAILs containing $FeCl_4^-$, $ZnCl_3^-$, $NiCl_3^-$ and $SnCl_3^-$ can be found in the SI along with the NMR spectra of the BAIL (**2**) (Figs. S1, S2, S3-S6). These confirmed the successful synthesis of the ILs. The

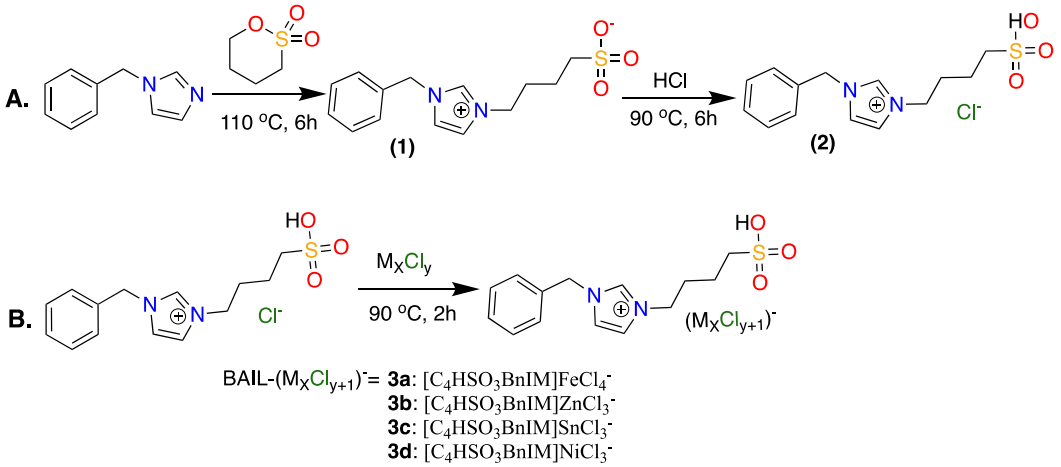

Scheme 2. Synthesis of (**A**) Brønsted Acidic Ionic liquids and (**B**) Brønsted-Lewis Acidic Ionic liquids.

viscosity of the BAIL (**2**) was measured to be 1068 mPa at 25 °C. The longer the alkyl chain, the higher the viscosity (Gao et al., 2024). Therefore, in comparison to ILs with simple structures, we anticipated a higher viscosity since this IL has a bulkier cation. Although the IL in this study is more sterically hindered, its viscosity is much lower than that of 1-pentyl-3-methylimidazolium iodide IL studied by Ruwaida et al. (Talip et al., 2021). The thermal gravimetric analysis trace in Fig. 1b shows an initial weight loss from 70 °C to 100 °C corresponding to the removal of surface-absorbed water and residual methanol solvents. Beyond solvent loss, BAIL **2** is thermally stable up to approximately 320 °C, after which a rapid decomposition event occurs. This is possibly because the organic cation decomposes, resulting in an 80 % weight loss. The remaining (10 % weight) materials present from 400 °C onwards likely correspond to inorganic residue with carbonaceous (char) matter (Amarasekara and Wiredu, 2014). The thermal stability of the BLAILs was also evaluated by TGA, revealing three main weight loss stages. The initial mass loss between 30 and 150 °C is attributed to the removal of adsorbed moisture and residual solvents. The materials remain thermally stable up to approximately 300 °C, after which the second degradation step occurs, possibly corresponding to the decomposition of the organic components of the BLAILs. The final weight loss observed above 400 °C is associated with the formation of thermally stable inorganic residues, confirming the successful incorporation of metal species. Since the decomposition of the ionic liquids begins above 300 °C, the ILs can be considered thermally stable under the catalytic reaction conditions, as the optimum reaction temperature is 170 °C. TGA was also used to analyze the spent catalyst's thermal behaviour, which showed several stages of decomposition. Desorption of residual solvents, volatile reaction products, and decomposition of adsorbed sugars (Fig. S15(B)) after catalyst reuse is responsible for the initial weight loss between 30 and 150 °C. Partial surface fouling during catalysis is indicated by the mass loss observed between 155 and 375 °C, which is attributed to the breakdown of remaining organic molecules, such as adsorbed sugars or chemical intermediates. The breakdown of the ionic liquid structure is linked to a significant deterioration process that is seen above 375 °C. The observed decrease in furfural yield following subsequent catalytic cycles is probably caused by the increasing structural degradation and surface fouling (Clarke et al., 2022)(Fig. S7). The FT-IR spectra of the BLAILS using pyridine as a probe are displayed in Fig. S8. This technique was used to ascertain the presence of both Brønsted and Lewis acidic sites in the ionic liquids (Dai et al., 2017). The FT-IR spectra of py-BLAILs featured two new distinct absorption peaks, 1450 cm^{-1} (Lewis acidic) and 1560 cm^{-1} (Brønsted acidic), in each of the spectra as compared to the spectrum of pure pyridine. The two distinct peaks were those of [py-H]+cation and the py-Lewis complex arising from the interactions of pyridine with the Brønsted and Lewis acidic centres, respectively (Liu et al., 2018a). From the spectra, we can conclude that the Brønsted-Lewis Acidic Ionic liquids (BLAILs) had both Brønsted and Lewis acidic centres, and these arise from the presence of sulfonic and metal complex anionic species present in the ILs (Liu et al., 2020).

The Brønsted acidity of the BAIL (**2**) in the form of Hammett acidity (H_0) was determined using UV–vis spectroscopy. The UV–vis spectra of 4-nitroaniline in an aqueous solution of BAIL (**2**) are shown in Fig. 1, and the H_0 value is in Table 1. The highest absorbance of the unprotonated form of the indicator was observed at 381; this absorbance decreased as the IL was added. The addition of the ILs to the indicator resulted in a decrease in absorbance, indicating their acidity. At 380 nm, the highest absorbance of the unprotonated form of the 4-nitroaniline indicator was recorded. However, when the acidic IL was added, the indicator was protonated by the acid, which then reduced the absorbance of the indicator, which was not protonated (Li et al., 2021; Suzuki et al., 2018). Therefore, adding an IL with strong acidity will result in a lower H_0 value. As seen from Table 1, the H_0 value of BAIL (**2**) was 1.058, possibly due to the sulfonic acidic moiety attached to the cation of the IL structure. The active proton in the sulfonic moiety contributes to the IL's acidic catalytic activity, according to Suzuki et al. (Aainaa et al., 2015; Li et al., 2021; Suzuki et al., 2018). The Hammett acidities of the Brønsted-Lewis acidic ILs were also determined to ascertain if the change in anions would affect the H_0 values (Table S1). The absorbance for the IL containing $FeCl_4^-$ was very high, hence the H_0 determination was inconclusive. This is because anions like these can form complexes that might affect the electrical environment of the IL, thereby altering the indicator's electronic transition and absorbances (Mero et al., 2022; Rai and Pandey, 2014). Furthermore, there is a discrepancy in the H_0 values of the ILs as compared to their Lewis acidities when the anions are $(M_xCl_{y+1})^-$ in this study. This is because H_0 measures Brønsted acidity, which deals with

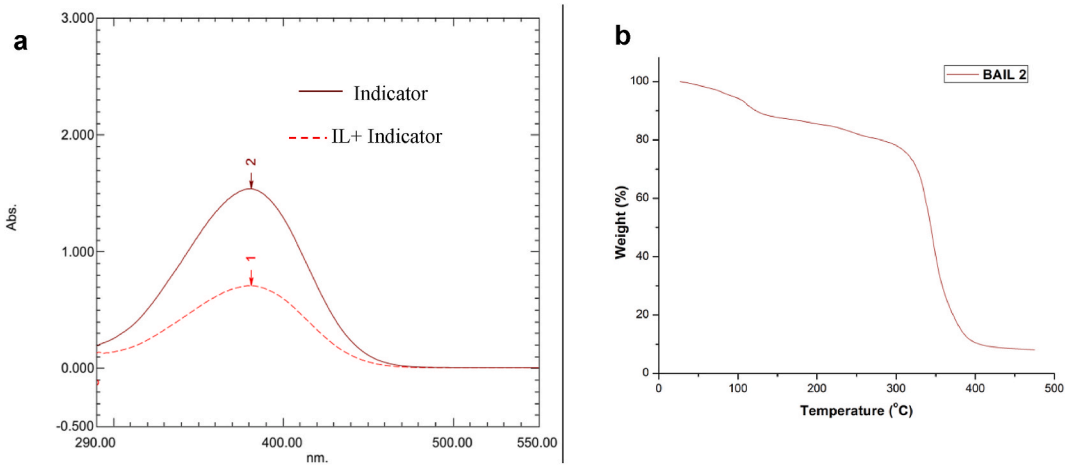

Figures (1a–b). (**a**) Absorption spectra for 4-nitroaniline in BAIL. (**b**) Thermal gravimetric analysis of BAIL **2.**

Table 1
Hammett acidity function calculation of ILs with different cations.

GRAPH LABEL	CONCENTRATION/mM	ABSORBANCE [AU]	[I%]	[IH^+%]	H_0
2	Blank-0.05 mM	1.537	100	0	–
1	[C_4HSO_3BnIM][Cl]0.36 mM	0.829	53.936	46.064	1.058

proton donation, whereas Lewis acidities deal with the acceptance of electron pairs. As stated earlier, there may be an interplay between charge transfers and solvent interactions, resulting in the deviation (Estager et al., 2014).

The green chemistry metrics related to BAIL (**2**) synthesis are shown in Table S2. The atom economy of the BAIL (**2**) synthesis was determined to be 100 % in both the zwitterion formation and the subsequent conversion to BAIL (**2**). This value is acceptable and indicates that no atoms were lost based on the reaction's stoichiometry. The E-factor for the BAIL (**2**) synthesis has been calculated to be 1.43, meaning that 1.43 g of waste was generated for every gram of the ionic liquid produced. The low reaction mass efficiency (RME) of 41.2 % can be attributed to the use of 30 % aqueous HCl, where the high water content contributes to the non-reactive mass. The final product yield decreases in relation to the total input mass due to the removal of excess water and HCl during the drying process. Thus, higher concentrations of reagents or better purification may allow greater efficiency. With a PMI of 2.43 g, BAIL (**2**) synthesis demonstrated effective material use that was within recognized ranges for lab-scale manufacture of fine chemicals (Sheldon, 2017). This means that 2.43 g was needed for each gram of product. Together with an E-factor of 1.43 and an RME of 41.2 %, this indicates moderate waste generation, likely due to excess water generated from the HCl used. Despite this, the procedure remains supported by metrics as a relatively scalable and eco-friendly approach for producing ILs (Constable et al., 2002).

2.3. Conversion of xylose and glucose with [C_4HSO_3BnIM][Cl^-] (BAIL 2)

The hydrolysis of cellulose and hemicellulose, represented by pure glucose and xylose, into the different platform chemicals, was carried out over 4 h at 170 °C and monitored by proton NMR. This also helped determine whether the source and formation of LA was from FFR or HMF. It is evident from the results that proton NMR peaks corresponding to FFR appear approximately one and a half hours after the xylose dehydration begins (Fig. 2). The reaction revealed that the IL proton NMR peaks remained constant, while the xylose proton NMR peaks decreased as the FFR proton NMR peaks appeared. This suggests that the IL catalyzes the reaction by forming hydrogen bonds with xylose, thus facilitating hydrolysis by donating an acidic proton (H^+) from its sulfonic group. The xylose dehydration results, including yields, turnover numbers (TONs), and catalyst loadings, were compared with those in the literature

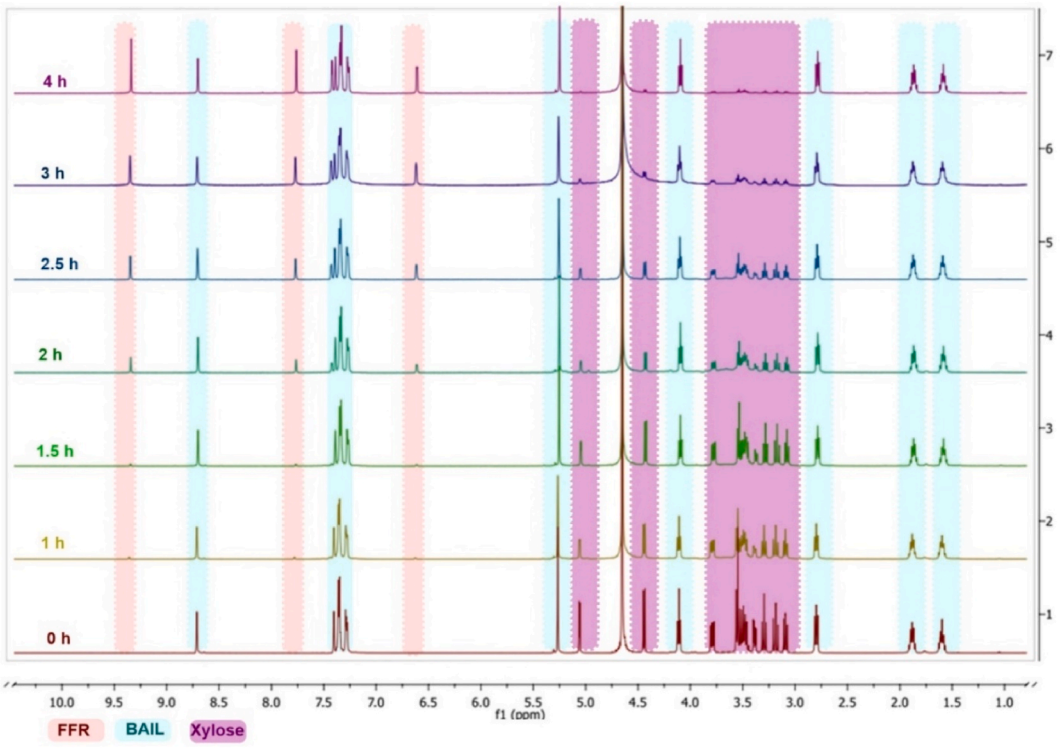

Fig. 2. Time-dependent dehydration of xylose; Conditions: Xylose (0.02 g), IL (0.019 wt%/0.036 mmol), water (6 mL), 4 h, 170 °C. ^{1}H NMR conducted at 25 °C in D_2O.

(Table S4). While high FFR yields (85 % and 80 %) were achieved with pyridinium ILs (Serrano-Ruiz et al., 2012; Xu et al., 2023), the catalyst efficiencies, reflected by moles of product per mole of catalyst (turnover number, TON), were significantly lower (TON = 1.61 and 4.73) than observed in this study (TON = 37) (Table S4 and Fig. 3a). An imidazolium IL (Table S4) reached 67.5 % FFR yield and a TON of 0.69 (Hua et al., 2021). In the glucose dehydration reaction, the HMF ^{1}H NMR peaks begin to form approximately 1 h after the reaction starts (Fig. S9a). At 2 h and 30 min, the LA proton NMR peaks appeared, while glucose was still present in solution. This suggests that glucose ↔ fructose isomerization occurs to a lesser extent, meaning further dehydration may necessitate a more isomerization-selective system and optimization. Prior studies on glucose conversion reported good HMF and LA yields using imidazolium ILs, requiring co-catalysts, albeit low catalyst efficiencies (TON = 1.78 and 0.20) were recorded (Table S5) (Aainaa et al., 2015; Kumar et al., 2021). $[C_4HSO_3BnIM][Cl]^-$ (BAIL **2**) efficiently produces HMF and LA, with satisfactory TON (TON = 5.8) and conversions (Fig. 3b–S9b). The proton NMR peaks corresponding to the IL catalyst remained unchanged during xylose and glucose conversion reactions, signifying stability and therefore good potential for recycling the IL in biphasic systems. Hence, reusing the same residual IL catalyst for subsequent reactions was pursued.

2.4. Conversion of corncobs to biochemicals using BAIL

After successfully dehydrating xylose and glucose, biomass derived from waste corn cobs was used as a feedstock to produce biochemicals at 170 °C, over 4 h, and initial biomass loadings [(0.6 g of biomass, 10 mL of water and 60 mL of toluene (0.12 g/0.36 mmol IL)]. Optimal conditions for the extraction, hydrolysis, and dehydration were determined by evaluating the effects of varying reaction parameters, which included time, temperature, stirring rate, catalyst loading, biomass loading, and the water: toluene solvent ratio.

2.5. Biomass conversion as a function of temperature and time

The reactions were carried out at temperatures ranging from 130 °C to 200 °C, and FFR yield increased with temperature from 15 % at 130 °C to 91 % at 170 °C (Fig. 4a). This is due to accelerated reaction rates from higher reactant-catalyst collisions and extraction rates as temperature increases. Notably, FFR yields decreased at 190 °C (86 %) and 200 °C (81 %), 21 possibly due to more huminic by-product formation. Humins are black particulate matter formed after polymerization and resinification of sugars, FFR and HMF- often causing catalyst deactivation and coking at elevated temperatures (Calderon et al., 2022). In contrast, neither HMF nor LA formed from 130 °C to 170 °C, although they did begin to form from 190 °C to 200 °C (Fig. 4c). Thus, using the same catalytic system, at lower temperatures maximizes FFR yield, while LA and HMF can be obtained at elevated temperatures. FFR yield improves over time (2 h, 44 % yield), leading to a 91 % FFR yield after 4 h (Fig. 4b). Further reaction of FFR beyond 4 h leads to resinification and humins formation, which deactivates the catalyst and reduces FFR yield, while HMF begins to form at this stage in low amounts (Fig. 4d). HMF to LA conversion is a multi-step reaction process (Árvai et al., 2024) involving glucose → isomerization to fructose, → then fructose dehydration to HMF, and HMF → rehydration to LA and formic acid. Therefore, it is not surprising that the LA output was lower than HMF due to inadequate reaction times and conditions. Additionally, as anticipated, the FFR yield was very poor (2.1 %) due to the omission of the catalyst, and LA was not produced. The zwitterionic species (**1**) in Scheme 2, as the catalyst, also granted low FFR yields (Table S3).

2.6. Effect of catalyst and biomass loading on biochemical yields

The availability of additional active catalytic sites from increasing the IL loading resulted in higher FFR yields of up to 91 % with (0.19 wt%/0.36 mmol) IL load. However, the FFR yield declined from 91 % to 85 % and further down to 66 % upon increasing the IL loading to 0.57 wt% (1.08 mmol) (Fig. 4e). This suggests that increased IL catalyst loading accelerates condensation or resinification

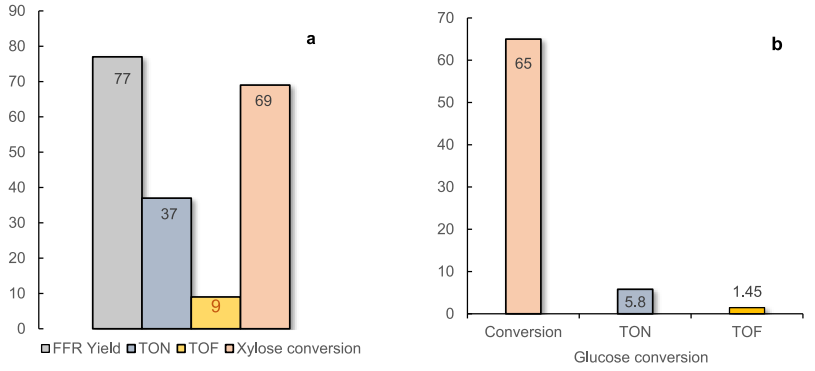

Figure (3a–b). Sugar dehydration: (**a**) xylose conversion to FFR and (**b**) glucose conversion. Conditions: Sugar (0.6 g), IL (0.19 wt%/0.36 mmol), D_2O (12 mL), 4 h, 170 °C. ^{1}H NMR calculated at 25 °C in D_2O using dimethylformamide as internal standard.

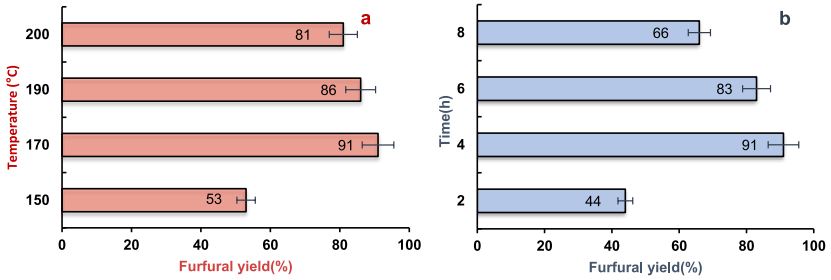

Figures (4a–b). Effect of: (**a**) Temperature in the extraction, conversion and separation of FFR, representative FFR yields are shown; Conditions: Reactions were carried out at 150 °C–200 °C over 4 h with (0.12 g/0.36 mmol) IL loading, 0.6 g corn cobs, 1400 rpm, water/toluene (1:6, 70 mL). (**b**) Time in the extraction, conversion and separation of FFR, representative FFR yields are shown; Conditions: Reactions were carried out for 2–8 h at 170 °C, with (0.12 g/0.36 mmol IL load), 0.6 g corn cobs, 1400 rpm, water/toluene (1:6, 70 mL). Yield calculated from ^{1}H NMR at 25 °C in $CDCl_3$ using dimethylformamide as an internal standard. FFR yields are calculated based on the hemicellulose content of the biomass feedstock.

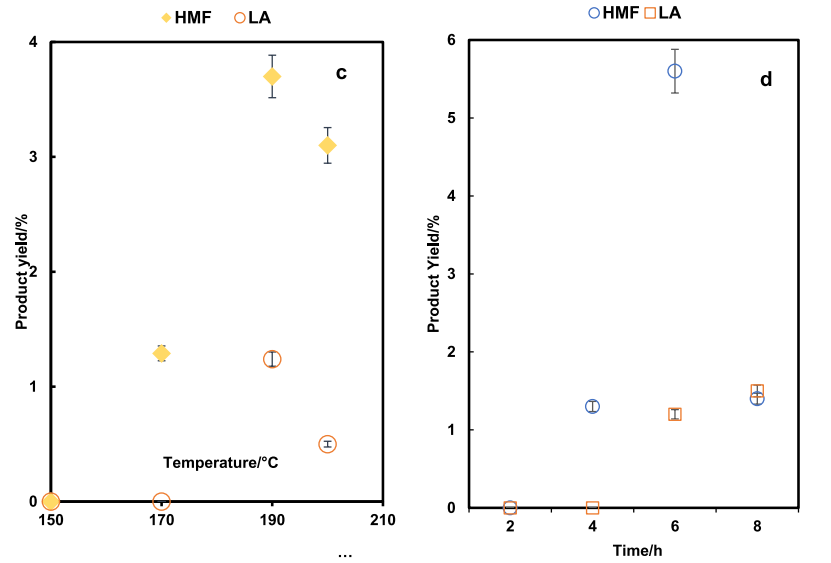

Figure (4c–d). Effect of (**c**) Temperature in the extraction, conversion and separation of HMF and LA, representative FFR yields are shown; Conditions: Reactions were carried out at 150 °C–200 °C, over 4 h with (0.12 g/0.36 mmol) IL loading, 0.6 g corn cobs, 1400 rpm, water/toluene (1:6, 70 mL). (**d**) Time in the extraction, conversion and separation of HMF and LA, representative yields are shown; Conditions: Reactions were carried out for 2–8 h at 170 °C, with (0.12 g/0.36 mmol IL load), 0.6 g corn cobs, 1400 rpm, water/toluene (1:6, 70 mL). LA and HMF yields are calculated based on the cellulose content of the biomass feedstock.

reactions between intermediates and/or the FFR, forming more huminic by-products. The HMF and LA production increased with increasing IL loading (working pH around 5), as seen in Fig. S9c. The highest HMF and LA yields were observed at an IL loading of 0.37 wt% (Liu et al., 2019). When a smaller amount of biomass was used, the FFR yield was lower because of less hemicellulose content in the biomass (Fig. 4f). Higher biomass loadings (0.9 g–1.2 g) did not increase yields as was anticipated, suggestive of mass transfer limitations at the solid (biomass) and liquid (aqueous IL catalyst) interface. Furthermore, increasing agitation speeds (1000–1600 rpm) enhances FFR yield (91 %, Fig. S10a), corroborating the existence of mass transfer limitations. Optimal agitation was established to be 1400 rpm. Increasing the biomass loading while maintaining the catalyst and solvent quantities resulted in a decrease in biochemicals production (Fig. 4f) (Fig. S9d). This clearly shows a dependence on the catalyst-to-substrate ratio of 1:5, so in a separate experiment, both the solvents and catalysts were increased proportionally with the biomass, maintaining a catalyst-to-substrate ratio of 1:5, which afforded up to a 91 % FFR yield (Fig. 4g) with its HMF and LA production shown in Fig. S11a. This proves the scalability of the process at a catalyst-to-substrate ratio of 1:5.

2.7. Solvent ratio and organic phase variation in the aqueous-biphasic system

The ideal biphasic composition was determined by varying the water: toluene ratio from 10:60 to 60:10 (v/v). Furfural yields

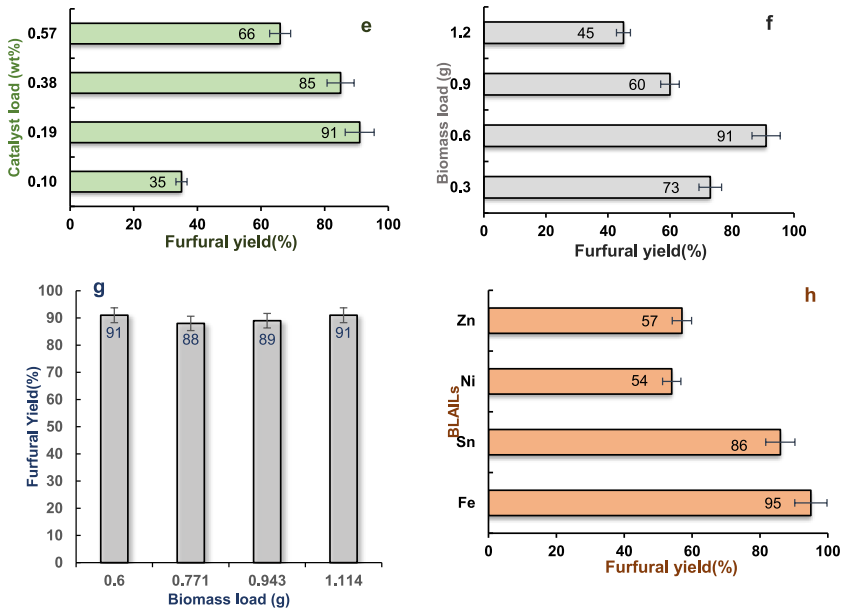

Figures (4e–h). Effect of (**e**) Ionic liquid loading in the extraction, conversion and separation of FFR, representative FFR yields are shown Conditions: Reactions were carried out with 0.10–0.57 wt%/0.18–1.08 mmol IL load at 170 °C for 4 h with 0.6 g corn cobs, 1400 rpm, water/toluene (1:6, 70 mL) (**f**) Biomass loading; Reactions were carried out with 0.3–1.2 g corn cob load at 170 °C for 4 h with 0.12 g IL, 1400 rpm, water/toluene (1:6, 70 mL).; Effect of (**g**) Upscaled catalyst and substrate; Conditions: Reactions were carried out for 4 h at 170 °C, with a C/S ratio of 1:5; IL loading ranging from 0.12 g to 0.23 g (0.36 mmol–0.69 mmol), with biomass loading ranging from 0.6 g to 1.114 g corn cobs, 1400 rpm, water/toluene (1:6, 70–130 mL): **(h)** BLAILs; Conditions: Reactions were carried out using optimum conditions of 170 °C, 4 h, 0.12g/0.36 mmol IL, 0.6 g corn cobs, 1400 rpm, water/toluene (1:6, 70 mL). Yield calculated from ^{1}H NMR at 25 °C in $CDCl_3$ using dimethylformamide as an internal standard.

significantly dropped with less toluene in the biphasic reaction medium, as seen in Fig. 5a. At 10:60, the dominant organic phase effectively removes furfural from the acidic aqueous layer, preventing rehydration and humin production, resulting in the maximum yield (Matsagar et al., 2017). On the other hand, furfural's residence time in the aqueous phase is prolonged by raising the water percentage, which encourages breakdown pathways and leads to noticeably reduced yield (Mittal et al., 2017). The organic co-solvent, in the aqueous biphasic media, enhances FFR yield by immediately transporting FFR as it is produced (from the aqueous acidic layer) into the neutral organic layer, thereby maximising yield. The results show toluene as an effective organic layer in the aqueous-biphasic system. Despite being effective, toluene is a fossil-based solvent (USEPA, 2005; Cheremisinoff and Rosenfeld, 2010). We, therefore, screened two bio-based solvents, 2-methylfuran (2-MF) and 2,5-dimethylfuran (2,5-DMF) as alternatives (Janicka et al., 2022). 2-MF performs marginally better than toluene, which in turn outperforms 2,5-DMF, likely due to reduced steric hindrance from the absence

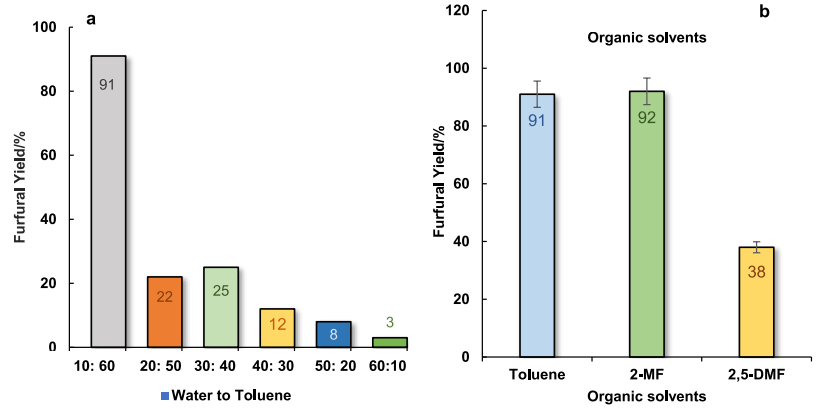

Figures (5a–b). Effect of (**a**) Water: Toluene ratio; Conditions: Reactions were carried out for 4 h at 170 °C, with a water to toluene ratio variation (10:60 to 60:10 v/v); IL loading of 0.12 g (0.36 mmol), 0.6 g corn cobs, 1400 rpm: (**b**): Effect of Different organic solvents; Conditions: Reactions were carried out with 0.6 g corn cob load at 170 °C for 4 h with 0.12 g IL, 1400 rpm, water/organic solvent (1:6, 10 mL).

of an extra methyl group in 2-MF and toluene (Avagyan et al., 2025) (Fig. 5b).

Overall, we found that BAIL **2** produces FFR (91 %) from raw biomass more efficiently when compared to prior reported systems (Table S6). For instance, 1-*n*-butyl-3-methyl-imidazole bromide, [BMIM][Br], produced 34 % and 59 % FFR, respectively, from rice husks and soy peel (Scapin et al., 2020). Again, [C_3HSO_3HMIM][HSO_4^-] with a Brønsted acid moiety converted sugarcane bagasse into a 73 % FFR (Matsagar et al., 2017). Scheme 1. To the best of our knowledge, [C_4HSO_3BnIM] [Cl] (BAIL **2**) used in a one-pot reaction system produced the highest yield of FFR from raw biomass, with the added benefit of pure FFR separation into the organic layer and also the simultaneous production of HMF and LA.

Prior reports on ILs for the production of LA and HMF show that [C_3SO_3HMIM][HSO_4] gave 96.6 mol% LA only from straw (Liu et al., 2018b), and [C_4MIM][HSO_4] resulted in 71 mol% LA from bamboo shoots (Zhou et al., 2013). Although the LA yields reported in this study are somewhat lower than the examples stated, the key advantage of our system is that it can generate multiple biochemicals simultaneously from raw biomass using very low catalyst load as compared to prior systems.

2.8. Conversion of corncobs and Arundo donax to biochemicals using BLAILs

Optimum reaction conditions obtained with BAIL **2** were applied to the hydrolysis reaction using BLAILs. The BLAIL containing the Fe^{3+} metal had a higher activity than the BAIL **2**, giving 95 % FFR yield (Fig. 4h). This improvement in the extraction, hydrolysis and dehydration of the hemicellulosic component of the biomass suggests a synergy between Brønsted and Lewis acidic sites. A plausible mechanism of action has been shown in Fig. S12 where the sulfonic proton and imidazolium C2–H in this dual acidic catalyst system give Brønsted acidity, which helps hydrolyze the β-1,4-glycosidic bonds in hemicellulose to release xylose. As described, the Lewis acids then facilitate an intramolecular 1,2-hydride shift that isomerizes xylose to xylulose. Furthermore, Lewis acids enhance the overall Brønsted acidity through synergistic interactions between Brønsted and Lewis acid sites (Zhao et al., 2019; Pan et al., 2022; Hui et al., 2019; Zhang et al., 2013). Higher metal charge density, as in Fe^{3+}, enhances Lewis acidity and electrophilicity. $FeCl_4^-$ also acts as a strong aqua acid, enhancing Lewis and Brønsted acidity. This promotes glucose isomerization to fructose, slightly increasing LA and HMF yields compared to reactions with BAIL (**2**) (Fig. S11b) (Huheey, 1972). The BLAIL containing the Fe^{3+} metal produced more HMF as compared to LA, while the BLAIL containing the Sn^{2+} converted more HMF to LA. The order of the catalytic activity of BLAILs in FFR production followed the trend Fe^{3+}>Sn^{2+}>Zn^{2+}>Ni^{2+}, which corresponds to the reported strength of Lewis acidity order (Huheey, 1972).

Despite the low FFR yield (46 %) (Fig. S10b), when BAIL **2** was used to convert giant cane (*Arundo donax*), likely due to its lower hemicellulose content, BLAILs catalytic activities were higher for giant cane, reaching 60 % with [C_4HSO_3BnIM][$SnCl_3^-$], and the order of activity was established as: Sn^{2+}> Fe^{3+}>Zn^{2+}>Ni^{2+} (Fig. S10b).

2.9. [C_4HSO_3BnIM][Cl] (BAIL 2) and [C_4SO_3BIM][$FeCl_4$] (BLAIL-Fe) recycling

After the reaction runs, the mixture is cooled, filtered to remove the biomass residue and the layers are separated to evaluate the recyclability of the [C_4SO_3BnIM][Cl] (BAIL **2**). FFR was found to be in the organic (toluene) layer while the HMF, LA and IL remained in the aqueous layer. After the removal of HMF and LA, the aqueous layer containing the IL was repurposed as the catalyst for the subsequent catalysis run by adding fresh toluene and biomass (Fig. S14). shows a ^{1}H NMR of isolated HMF and LA from a hydrolysis reaction. Recyclability studies were investigated for the production of FFR only due to its high initial output as compared to LA and HMF. It is evident from the data that FFR was still produced by the reaction following the first run, but after the second run, the FFR yield decreased from 91 % to 72 %. The fourth run afforded a 57 % FFR yield (Fig. 6). Despite the employment of a biphasic system to inhibit the emergence of humins, the reduced FFR yield may have been caused by some soluble humic materials from the first catalysis run, which persisted in the aqueous layer and hence influenced the subsequent catalysis runs. The TGA of the BAIL **2** shows that it is thermally stable and only starts to degrade after 250 °C, the ^{1}H NMR spectra (Figure S15 (B)) of the aqueous layer after the removal of HMF and LA demonstrates the integrity of the IL as evidenced by the presence of BAIL (**2**) ^{1}H NMR signals. TGA was also used to

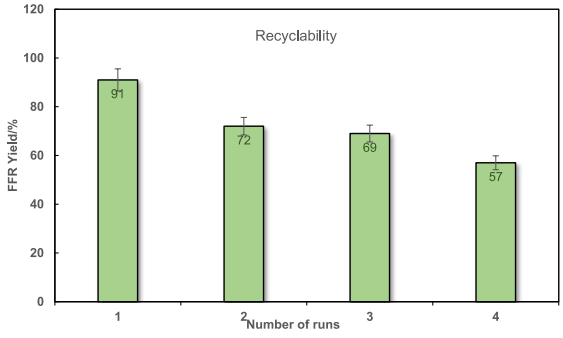

Fig. 6. Recycling tests of [C_4SO_3BIM][Cl]; Conditions: 0.6 g corn cob load at 170 °C for 4 h with 0.12 g IL, water: toluene solvent(10:60 mL). ^{1}H NMR in $CDCl_3$ using dimethylformamide as an internal standard. FFR yields are calculated based on the hemicellulose content of the biomass.

analyze the spent catalyst's thermal behavior, which showed several stages of decomposition. Desorption of residual solvents and decomposition of adsorbed sugars (see Fig. S15(B)) after catalyst reuse is responsible for the initial weight loss between 30 and 150 °C. Partial surface fouling during catalysis is shown by the following mass loss between 155 and 375 °C, which is associated with the breakdown of remaining organic molecules, such as adsorbed sugars or chemical intermediates. The breakdown of the ionic liquid structure is linked to a significant deterioration process that is seen above 375 °C. The observed decrease in furfural yield following subsequent catalytic cycles is caused by this increasing structural degradation and surface fouling (Xu and Cheng, 2021) (Fig. S13b). The recyclability for the best performing $[C_4SO_3BnIM][Cl–FeCl_3]$ (BLAIL-Fe) was tested solely for FFR synthesis from corn cobs. The FFR yield decreased from 95 % to 71 mol% in the second run and was maintained in the third run, however, the FFR yield further dropped from 71 % to 50 % and finally to 42 % as seen in Fig. S13a.

2.10. Analysis of untreated and post-reaction biomass residue

The X-ray diffractograms of the waste biomass before and after hydrolysis (residue) are shown in Fig. 7. The diffractograms reveal the presence of natural cellulose I polymorph having three distinct peaks at (1 $\bar{1}$ 0),(110), (040) and (200) (French, 2014), with the largest peak at 22 corresponding to the (200) plane and the final minor peak around 35 corresponding to the (040) plane (Kljun et al., 2011; Ju et al., 2015). Using Segel's equation, the crystallinity index for the residue and raw corn cobs was determined to be 37.4 % and 21.8 %, respectively. Indicated by the residue's higher crystallinity index, the depolymerization of amorphous hemicellulose produced a more crystalline cellulose pulp (Fig. 7).

Furthermore, the structural morphology of the raw and hydrolyzed biomass in Fig. S16 showed that the raw biomass had a smoother, more intact surface compared to the residue's rough surface, which featured numerous fissures (Sun et al., 2020). Under acidic conditions, lignocellulosic biomass is known to lose its intricate structure; the lignin shell breaks down and exposes the holocellulose-rich interior, enabling the IL to degrade the hemicellulose content with minimal breakdown of the cellulosic content (Mamilla et al., 2019).

Additionally, the post-hydrolysis biomass residue's FT-IR spectra were examined and contrasted with those of pure cellulose. The bands of intra- and intermolecular hydrogen bonds, as well as the valence bands of the O–H group's hydrogen bond, vibrates at 3321 cm^{-1} and is caused by the crystalline structure of cellulose (Fig. S17). Moreover, the peak at 2893 cm^{-1} corresponding to cellulose properties is due to the asymmetric stretching of CH_2 and CH (Apaydın Varol and Mutlu, 2023). There were also a few peaks typical of lignin, located around 1598 cm^{-1}, 1512 cm^{-1} and 1289 cm^{-1} (Rashid et al., 2016). The SEM and NMR results are in agreement with the fact that FFR was solely produced from the hemicellulosic content of the biomass, as corroborated by the fact that under the optimum reaction conditions, pure cellulose did not form FFR when used as a substrate for hydrolysis, as seen in the proton NMR of the organic layer, where we expect to find FFR (Fig. S18). As demonstrated by pure glucose hydrolysis, LA was generated only from the cellulosic content (Fig. S9a). This suggests ILs mainly depolymerize hemicellulose, leaving behind a rich cellulosic pulp which is like microcrystalline cellulose (MCC). MCC is a multifunctional material with applications across various industries (Queiroz et al., 2021; Lupidi et al.; Asif et al., 2022).

2.11. Green chemistry metrics for BAIL 2 promoted corn cobs conversion to furfural

The use of green chemistry principles as well as metrics is important to chemists and chemical engineers for developing safer and more sustainable processes and products (Akakios et al., 2021; Trost, 1991). We addressed green metrics such as atom economy, Environmental factor (E-factor) and Product Mass Intensity (PMI) for the herein reported biorefinery process. A measurement of the molecular weight of the desired product in relation to the total molecular weight of all the species derived from the stoichiometric reaction equation – that is, the Atom economy assessment (Trost, 1991) (Table S2). The Atom Economy of FFR production was 64.01 %, which is less than 100 % due to possible side reactions like the formation of humins. This value is consistent with data reported by Dusselier et al. (2014) for furfural formation. Because the process was solvent-intensive, the E-factor determined as the simple E−factor (sEF), without solvents, was 1.805, but the total E-factor, which included solvents, was much higher at 85.46. Product mass intensity (PMI) was used as a measure of the total weight of all raw materials (including solvents and water) needed for the synthesis. The PMI was estimated at 86.48, mostly because of the large volumes of solvent (common in lab-scale biorefinery processes) used compared to the amount of product. This value, *albeit* high, takes into consideration the loss of water and partial recovery of toluene. The recyclability of the IL and toluene lessens the environmental impact, highlighting the necessity to consider PMI in conjunction with other green metrics for a fair assessment of process sustainability. We also assessed the process using the reaction mass efficiency (RME) to gain a supplementary perspective on its efficiency and greenness (Andraos, 2005). The RME was found to be 58.21 %, which falls within the typical range for acid hydrolysis reactions and suggests good material utilization (Curzons et al., 2001).

3. Conclusion

In summary, waste corn cobs and *Arundo donax* were hydrolyzed in a one-pot system using imidazolium ILs $[C_4SO_3BnIM][Cl]$, resulting in higher yields of FFR than previously reported (91 % and 46 %, respectively). In addition to FFR, the ionic liquids were also able to hydrolyze the cellulose and generate glucose, which isomerizes to fructose and dehydrates to form HMF, an intermediate that produces LA. Furthermore, when the catalytic activity of the synthesized BLAILS was evaluated using corn cobs as feedstock, the BLAIL containing $FeCl_3$ produced a 95 % FFR yield. This demonstrates how the Brønsted and Lewis acid centres work in harmony. Despite the

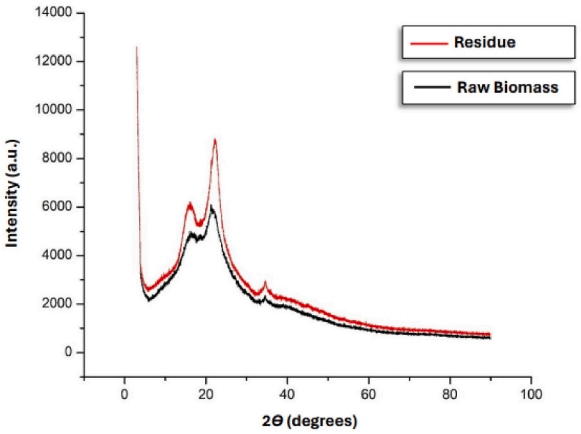

Fig. 7. Powder X-ray diffraction of raw biomass and residue.

low yields, it has been determined that the BAIL not only targets the hemicellulosic portion of biomass but also can break down the cellulose into other significant platform chemicals like LA and HMF. Compared to FFR, LA requires more severe reaction conditions to be produced. Consequently, a two-stage procedure or a flow system might be used to maximize the yields of both products, such that the FFR produced does not deteriorate into humins. This would allow the removal of FFR once generated and give way for the remaining cellulose to hydrolyze under harsher conditions. The direct one-pot synthesis of FFR, LA and HMF from waste biomass has been made possible by the catalytic efficiency of the IL [C_4SO_3BnIM][Cl]. This implies that in certain contexts, the versatility of this IL can provide a practical alternative to multi-step processing.

CRediT authorship contribution statement

Winifred D. Anyomih: Writing – original draft, Methodology, Investigation, Formal analysis, Data curation. **James Darkwa:** Writing – review & editing, Supervision, Resources, Project administration. **Paseka T. Moshapo:** Writing – review & editing, Validation, Supervision, Project administration. **Gift Mehlana:** Visualization, Software, Formal analysis, Data curation. **Banothile C.E. Makhubela:** Writing – review & editing, Validation, Supervision, Resources, Project administration, Funding acquisition.

Declaration of competing interest

The authors declare that they have no known competing financial interests or personal relationships that could have appeared to influence the work reported in this paper.

Acknowledgements

We acknowledge funding provided by the National Research Foundation of South Africa (Grant No. SRUG22052514577), the UJ Research Centre for Synthesis and Catalysis (RCSC). We are also grateful to the University of Johannesburg (UJ) and UJ Spectrum (Faculty of Science) for access to NMR and SEM, PXRD instruments and access to research infrastructure.

Appendix A. Supplementary data

Supplementary data to this article can be found online at https://doi.org/10.1016/j.scp.2026.102315.

Data availability

Data will be made available on request.

References

Aainaa, N., Ramli, S., Aishah, N., Amin, S., 2015. J. Mol. Catal. Chem. 407, 113–121.
Ahmad, F.B., Kalam, M.A., Zhang, Z., Masjuki, H.H., 2022. Energy Convers. Manag. X 14, 1–23.
Akakios, S.G., Bode, M.L., Sheldon, R.A., 2021. Green Chem. 23, 3334–3347.
Amarasekara, A.S., 2016. Chem. Rev. 116, 6133–6183.
Amarasekara, A.S., Wiredu, B., 2014. Sustain. Energy 2, 102–107.

Andraos, J., 2005. Org. Process Res. Dev. 9, 149–163.
Apaydın Varol, E., Mutlu, Ü., 2023. Energies 16, 1–19.
Arias, K.S., Velty, A., Climent, M.J., Iborra, S., 2024. Tetrahedr. Green Chem. 3, 1–13.
Árvai, C., Medgyesi, Z., Lui, M.Y., Mika, L.T., 2024. Adv. Synth. Catal. 366, 4846–4888.
Asif, M., Ahmed, D., Ahmad, N., Qamar, M.T., Alruwaili, N.K., Bukhari, S.N.A., 2022. Polymers (Basel) 14.
Avagyan, N.A., Zonov, R.V., Lemport, P.S., Evsiunina, M.V., Matveev, P.I., Roznyatovsky, V.A., Averin, A.D., Kalle, P., Tafeenko, V.A., Soloveva, S.A., Nelyubina, Y.V., Petrov, V.G., Ustynyuk, Y.A., Nenajdenko, V.G., 2025. Dalton Trans. 1–13.
Calderon, J.C., Arora, J., Mushrif, S., 2022. ACS Omega 7, 44786–44795.
Chang, J.C., Yang, C.H., Sun, I.W., Ho, W.Y., Wu, T.Y., 2018. Materials (Basel) 11, 1–12.
Cheng, X., Liu, Y., Wang, K., Yu, H., Yu, S., Liu, S., 2021. Catal. Lett. 1–12.
Cheremisinoff, N.P., Rosenfeld, P.E., 2010. In: Handbook of Pollution Prevention and Cleaner Production. Elsevier, pp. 179–259.
Clarke, C.J., Baaqel, H., Matthews, R., Chen, Y., Lovelock, K., Hallett, J.P., Licence, P., 2022. Green Chem. 24, 5800–5812.
Constable, D.J.C., Curzons, A.D., Cunningham, V.L., 2002. Green Chem. 4, 521–527.
Costa, S.P.F., Azevedo, A.M.O., Pinto, P.C.A.G., Saraiva, M.L.M.F.S., 2017. ChemSusChem 10, 2321–2347.
Curzons, A.D., Constable, D.J.C., Mortimer, D.N., Cunningham, V.L., 2001. Green Chem. 3, 1–6.
Dai, L., Zhao, Q., Fang, M., Liu, R., Dong, M., Jiang, T., 2017. RSC Adv. 7, 32427–32435.
de Jong, E., Stichnothe, H., Bell, G., Jørgensen, H., 2020. Bio-Based Chemicals. IEA Bioenergy.
Dusselier, M., Mascal, M., Sels, B.F., 2014. Top. Curr. Chem. 544, 1–41.
Estager, J., Holbrey, J.D., Swadźba-Kwaśny, M., 2014. Chem. Soc. Rev. 43, 847–886.
Fliegar, J., Flieger, M., 2020. Int. J. Mol. Sci. 21, 1–41.
French, A.D., 2014. Cellulose 21, 885–896.
Gao, N., Yang, Y., Wang, Z., Guo, X., Jiang, S., Li, J., Hu, Y., Liu, Z., Xu, C., 2024. Chem. Rev. 124, 27–123.
Green, M.D., Long, T.E., 2009. Polym. Rev. 49, 291–314.
Greer, A.J., Jacquemin, J., Hardacre, C., 2020. Industrial Applications of Ionic Liquids, 25.
Guo, X., Guo, F., Li, Y., Zheng, Z., Xing, Z., Zhu, Z., Liu, T., Zhang, X., Jin, Y., 2018. Appl. Catal. Gen. 558, 18–25.
Haldar, D., Dey, P., Thomas, J., Singhania, R.R., Patel, A.K., 2022. Bioresour. Technol. 365, 128180.
Hayes, D.J., Fitzpatrick, S., Hayes, M.H.B., Ross, J.R.H., 2006. In: Biorefineries–Industrial Processes and Products: Status Quo and Future Directions, 29, pp. 139–163.
Hu, W., Xu, H., Zhang, Z., Duan, Y., Lu, X., Lu, L., Si, C., Peng, Y., Li, X., 2024. Biomass Bioenergy 186, 107275.
Hua, D., Ding, H., Liu, Y., Li, J., Han, B., 2021. Catalysts 11, 1–8.
Huang, L., Peng, H., Xiao, Z., Wu, H., Fu, G., Wan, Y., Bi, H., 2022. Ind. Crops Prod. 184, 1–11.
Huheey, J.E., 1972. In: Inorganic Chemistry: Principles of Structure and Reactivity, pp. 214–215.
Hui, W., Zhou, Y., Dong, Y., Cao, Z.J., He, F.Q., Cai, M.Z., Tao, D.J., 2019. Green Energy Environ. 4, 49–55.
Janicka, P., Płotka-Wasylka, J., Jatkowska, N., Chabowska, A., Fares, M.Y., Andruch, V., Kaykhaii, M., Gębicki, J., 2022. Curr. Opin. Green Sustainable Chem. 37, 1–11.
Ju, X., Bowden, M., Brown, E.E., Zhang, X., 2015. Carbohydr. Polym. 123, 476–481.
Kapanji, K.K., Haigh, K.F., Görgens, J.F., 2021. Biomass Bioenergy 146, 1–8.
Karami, S., Momeni, A.R., Albadi, J., 2019. Res. Chem. Intermed. 45, 3395–3408.
Karinen, R., Vilonen, K., Niemelä, M., 2011. ChemSusChem 4, 1002–1016.
Kljun, A., Benians, T.A.S., Goubet, F., Meulewaeter, F., Knox, J.P., Blackburn, R.S., 2011. Biomacromolecules 12, 4121–4126.
Kumar, K., Pathak, S., Upadhyayula, S., 2020. J. Clean. Prod. 256, 120292.
Kumar, K., Kumar, M., Upadhyayula, S., 2021. Molecules 26, 1–14.
Kumar, S., Choudhary, P., Sharma, D., Sajwan, D., Kumar, V., Krishnan, V., 2024. ChemSusChem 17, 1–52.
Lange, J.P., Wadman, S.H., 2020. ChemSusChem 13, 5329–5337.
Li, M., Chen, J., Li, L., Ye, C., Lin, X., Qiu, T., 2021. Green Energy Environ. 6, 271–282.
Li, X., Cong, H., Zhao, W., Yang, S., Li, H., 2024. ChemSusChem 18, 1–9.
Liu, S., Tan, S., Bian, B., Yu, H., Wu, Q., Liu, Z., Yu, F., Li, L., Yu, S., Song, X., Song, Z., 2018a. RSC Adv. 8, 19551–19559.
Liu, L., Li, Z., Hou, W., Shen, H., 2018b. Carbohydr. Polym. 181, 778–784.
Liu, S., Wang, K., Yu, H., Li, B., Yu, S., 2019. Sci. Rep. 9, 1–9.
Liu, Y., Wu, Y., Su, M., Liu, W., Li, X., Liu, F., 2020. J. Ind. Eng. Chem. 92, 200–209.
Liu, Y., Forster, L., Mavridis, A., Merenda, A., Ahmed, M., D'Agostino, C., Konarova, M., Seeber, A., Della Gaspera, E., Lee, A.F., Wilson, K., 2024. ChemSusChem 202401494, 1–16.
G. Lupidi, G. Pastore, E. Marcantoni and S. Gabrielli, Molecules, , DOI:10.3390/molecules28052009.
Mamilla, J.L.K., Novak, U., Grilc, M., Likozar, B., 2019. Biomass Bioenergy 120, 417–425.
Matsagar, B.M., Dhepe, P.L., 2017. New J. Chem. 41, 6137–6144.
Matsagar, B.M., Hossain, S.A., Islam, T., Alamri, H.R., Alothman, Z.A., Yamauchi, Y., Dhepe, P.L., Wu, K.C.W., 2017. Sci. Rep. 7, 1–7.
Mero, A., Guglielmero, L., Guazzelli, L., D'Andrea, F., Mezzetta, A., Pomelli, C.S., 2022. Molecules 27, 1–15.
Mittal, A., Black, S.K., Vinzant, T.B., O'Brien, M., Tucker, M.P., Johnson, D.K., 2017. ACS Sustain. Chem. Eng. 5, 5694–5701.
Nie, Y., Hou, Q., Li, W., Bai, C., Bai, X., Ju, M., 2019. Molecules 24, 1–18.
Oklu, N.K., Matsinha, L.C., Makhubela, B.C.E., 2020. Solvents, Ion. Liq. Solvent Eff. 1–24.
Olivares, Y., Herrera, C., Seguel, J., Sepúlveda, C., Parra, C., Pecchi, G., 2023. Catalysts 13, 1–15.
Pan, A., Chojnacka, M., Crowley, R., Gottermann, L., Haines, B., Kou, K., 2022. Chem. Sci. 13, 3539–3548.
Queiroz, A.L.P., Kerins, B.M., Yadav, J., Farag, F., Faisal, W., Crowley, M.E., Lawrence, S.E., Moynihan, H.A., Healy, A.M., Vucen, S., Crean, A.M., 2021. Cellulose 28, 8971–8985.
Radhakrishnan, R., Patra, P., Das, M., Ghosh, A., 2021. Renew. Sustain. Energy Rev. 149, 1–20.
Rai, R., Pandey, S., 2014. J. Phys. Chem. B 118, 11259–11270.
Ramli, N.A.S., Amin, N.A.S., 2017. Bioenergy Res. 10, 50–63.
Rashid, T., Kait, C.F., Murugesan, T., 2016. Procedia Eng. 148, 1312–1319.
Ren, H., Zhou, Y., Liu, L., 2013. Bioresour. Technol. 129, 616–619.
Scapin, E., Rambo, M.K.D., Viana, G.C.C., Marasca, N., Lacerda, G.E., Rambo, M.C.D., de, R., Fernandes, M.N., 2020. Food Sci. Technol. 40, 83–87.
Segers, B., Nimmegeers, P., Spiller, M., Tofani, G., Jasiukaityte-Grojzdek, E., Dace, E., Kikas, T., Marchetti, J.M., Rajic, M., Yildiz, G., Billen, P., 2024. RSC Sustain. 2, 3730–3749.
Serrano-Ruiz, J.C., Campelo, J.M., Francavilla, M., Romero, A.A., Luque, R., Menéndez-Vázquez, C., García, A.B., García-Suárez, E.J., 2012. Catal. Sci. Technol. 2, 1828–1832.
Sheldon, R.A., 2017. Green Chem. 19, 18–43.
Shuai, L., Luterbacher, J., 2016. ChemSusChem 9, 133–155.
J. K. Singh, R. K. Sharma, P. Ghosh, A. Kumar and M. L. Khan, Front. Chem., , DOI:10.3389/fchem.2018.00548.
Sun, S., Cao, X., Huiling, L., Yingbo, Z., Yijing, L., Wei, J., Yang, W., Shaoni, S., 2020. Polymers (Basel). 12, 1–13.
Suzuki, S., Takeoka, Y., Rikukawa, M., Yoshizawa-Fujita, M., 2018. RSC Adv. 8, 14623–14632.
Talip, R.A.A., Yahya, W.Z.N., Bustam, M.A., 2021. E3S Web Conf. 287, 8–11.

Thanheuser, N., Groteguth, J.T., Leitner, W., Esteban, J., Vorholt, A.J., 2024. ChemSusChem 18, 1–9.
Topias Kilpinen, A., Yousefi, N., Kontturi, E., 2024. ChemSusChem 202401291, 1–7.
Torres-Olea, B., Pérez-Merchán, A., Díaz-Maizkurrena, P., Requies, J.M., Moreno-Tost, R., Cecilia, J.A., García-Sancho, C., Maireles-Torres, P., 2024. Catal. Today 427, 1–13.
Tran, P.H., Duy Nguyen, A.T., Nguyen, H.T., Le, T.N., 2017. RSC Adv. 7, 54399–54406.
Trost, B., 1991. Science 254, 1471–1477 (80-).
USEPA, 2005. Toxicological Review of Toluene (CAS No. 108-88-3), Washington.
Vojtova, I., Leinweber, P., Weidlich, T., 2024. Catalysts 14, 1–29.
Wang, Y., Dai, Y., Wang, T., Li, M., Zhu, Y., Zhang, L., 2022. Fuel Process. Technol. 237, 1–9.
Weingarten, R., Tompsett, G.A., Conner, W.C., Huber, G.W., 2011. J. Catal. 279, 174–182.
Wu, M., Lui, W., Deng, F., Lui, S., Song, K., He, J., Li, H., 2024. ChemSusChem, e202402165, 1–13.
Xia, Q., Peng, H., Zhang, Y., Fu, G., Liu, Y., Xiao, Z., Huang, L., Bi, H., 2023. Biomass Convers. Biorefinery 13, 7895–7907.
Xu, C., Cheng, Z., 2021. Processes 9, 1–36.
Xu, G., Tu, Z., Hu, X., Li, M., Zhang, X., Wu, Y., 2023. Fuel 339, 1–8.
Yao, L., Liu, S., Li, L., Yu, S., Lui, F., Song, Z., 2016. Bull. Chem. Soc. Ethiop. 30, 283–288.
You, S.J., Kim, Y.T., Park, E.D., 2014. React. Kinet. Mech. Catal. 111, 521–534.
Zhang, L., Yu, H., Wang, P., Dong, H., Peng, X., 2013. Bioresour. Technol. 130, 110–116.
Zhang, X., Zhang, X., Sun, N., Wang, S., Wang, X., Jiang, Z., 2019. Renew. Energy 141, 802–813.
Zhao, Y., Xu, H., Lu, K., Qu, Y., Zhu, L., Wang, S., 2019. Energy Sci. Eng. 7, 2237–2246.
Zhou, C., Yu, X., Ma, H., He, R., Vittayapadung, S., 2013. Chin. J. Chem. Eng. 21, 544–550.